Effects of Single-Tryptophan Mutations on R67 Dihydrofolate Reductase†

Freddie W. West,‡ Han-Seok Seo,‡ Thomas D. Bradrick,§ and Elizabeth E. Howell*,‡

Department of Biochemistry, Cellular and Molecular Biology, University of Tennessee, Knoxville, Tennessee 37996-0840, and Optical Spectroscopy Section, National Heart, Lung and Blood Institute, National Institutes of Health, Bethesda, Maryland 20892-1412

Received September 22, 1999; Revised Manuscript Received January 6, 2000

ABSTRACT: R67 dihydrofolate reductase (DHFR) is an R-plasmid-encoded enzyme that confers clinical resistance to the antibacterial drug trimethoprim. This enzyme shows no sequence or structural homology to the chromosomal DHFRs. The active form of the protein is a homotetramer possessing D_2 symmetry and a single active-site pore. Two tryptophans occur per monomer: W38 and its symmetry-related residues (W138, W238, and W338) occur at the dimer−dimer interfaces, while W45 and its symmetry-related partners (W145, W245, and W345) occur at the monomer−monomer interfaces. Two single-tryptophan mutant genes were constructed to determine the structural and functional consequences of four mutations per tetramer. The W45F mutant retains full enzyme activity and the fluorescence environment of the unmutated W38 residues clearly monitors ligand binding and a pH dependent tetramer ⇌ 2 dimers equilibrium. In contrast, four simultaneous W38F mutations at the dimer−dimer interfaces result in tetramer destabilization. The ensuing dimer is relatively inactive, as is dimeric wild-type R67 DHFR. A comparison of emission spectra indicates the fluorescent signal of wild-type R67 DHFR is dominated by the contribution from W38. Equilibrium unfolding/folding curves at pH 5.0, where all protein variants are dimeric, indicate the environment monitored by the W38 residue is slightly less stable than the environment monitored by the W45 residue.

Protein association, folding, and ligand binding can frequently be monitored by fluorescence spectroscopy as the intrinsic chromophore, tryptophan, is sensitive to the polarity of its environment. Fluorescence measurements are multidimensional as the signals include fluorescence intensity (at some emission wavelength emλ), $F_{em\lambda}$; quantum yield, Φ; emission maximum, λ_{max}; fluorescence lifetime, τ_1; preexponential factor, α_1; fluorescence anisotropy, r; and rotational correlation time, ϕ (*1*). This multidimensionality enhances the effectiveness of fluorescence as a tool, since it is likely that one of these signals will be sensitive to the conformational state of the protein.

The unambiguous assignment of the fluorescence properties to an individual tryptophan residue is necessary to interpret the observed fluorescence signals at a molecular level. If there are several tryptophans dispersed throughout the protein structure, it is difficult to resolve individual contributions, limiting the ability to interpret the structural and dynamic properties of these side chains (*1*). To overcome this limitation, site-directed mutagenesis can be used to construct single-tryptophan-containing mutants (*2*−*10*). Typically, tryptophans are replaced with the weakly fluorescent amino acid phenylalanine.

In R67 dihydrofolate reductase (DHFR),[1] tryptophan fluorescence has been quite useful in monitoring a variety of structural and functional properties. These include observing ligand binding, a pH-dependent dissociation of active homotetramer to relatively inactive dimers and protein folding (*11*−*14*). Since R67 DHFR possesses two tryptophans per monomer, the individual contributions of each tryptophan to a particular process have not been delineated. This research describes the construction and characterization of two single-tryptophan mutants in R67 DHFR.

R67 DHFR is an R-plasmid encoded enzyme that confers resistance to the antibacterial drug trimethoprim upon host bacteria. R67 DHFR is interesting as it shows no sequence or structural homology to chromosomal or other R-plasmid-encoded DHFRs (*15*, *16*). It also is one of the smallest monomers (78 amino acids) known to assemble into a catalytically active protein. Crystal structures of a relatively inactive dimer and of the active homotetramer have been described (*15*, *17*). Each monomer is a five-stranded β-barrel that is not stable in isolation. Association of two monomers to dimer occurs by formation of an intersubunit β-barrel. Two dimers then associate to form active tetramer. Each dimer−dimer interface is stabilized by interactions between the loop connecting β-strands c and d (residues 60−65) and four amino acids preceding β-strand b (residues 36−39). Figure 1 depicts the tetramer structure.

† This research was supported by NIH Grant GM35308 and NSF Grant MCB-9808302 (to E.E.H.). T.D.B. was supported by a postdoctoral fellowship from the National Institute of Neurological Disorders and Stroke, National Institutes of Health (NIH).

* Corresponding author: phone 865-974-4507; fax 865-974-6306; email lzh@utk.edu.

‡ University of Tennessee.

§ NIH.

[1] Abbreviations: DHFR, dihydrofolate reductase; wt, wild type; TMP, trimethoprim; DHF, dihydrofolate, NADP(+/H), nicotinamide adenine dinucleotide phosphate (oxidized/reduced); MTA buffer, 100 mM Tris, 50 mM MES, 50 mM acetic acid, and 10 mM β-mercaptoethanol polybuffer; CD, circular dichroism; GdnHCl, guanidine hydrochloride. Mutant enzymes containing amino acid substitutions are described by the wild-type residue and numbered position in the sequence, followed by the amino acid substitution. For example, W38F R67 DHFR describes the Trp-38 → Phe mutant.

10.1021/bi992195x CCC: $19.00
Published on Web 03/07/2000

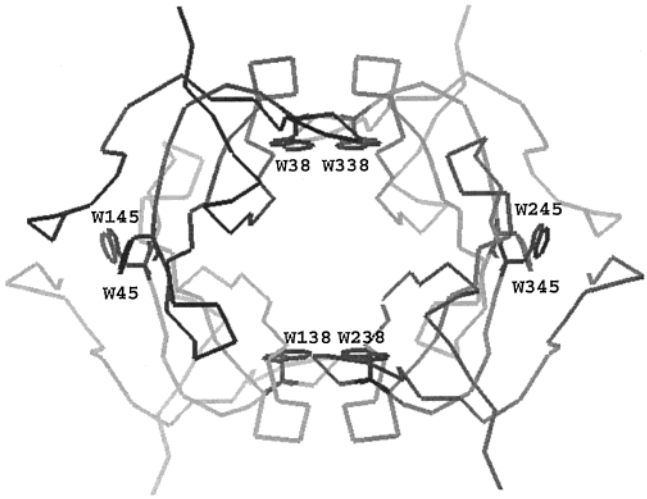

FIGURE 1: Crystal structure of tetrameric R67 DHFR. W38 and its symmetry-related partners (W138, W238, and W338) occur at the dimer−dimer interfaces (at the top and bottom of the figure), while W45 and its symmetry-related partners (W145, W245, and W345) occur at the monomer−monomer interfaces (to the left and right in the figure). The active-site pore can be viewed in the center.

Dissociation of active tetramer to two relatively inactive dimers occurs at pH < 7 upon protonation of H62 and its symmetry-related residues[2] (H162, H262, and H362; *12*). Thus the association state of R67 DHFR varies as a function of pH. As W38 and its symmetry related partners (W138, W238, and W338) also occur at the dimer−dimer interfaces, their environment should monitor the association state of R67 DHFR (see Figure 1). Similarly, since W45, W145, W245, and W345 occur at the monomer−monomer interfaces, their environment might be expected to predominantly monitor folding/unfolding in dimeric R67 DHFR since equilibrium folding/unfolding curves are readily fit by the two state model, dimer ⇌ 2 unfolded monomers (*11*).

Tetrameric R67 DHFR assembles as a toroid, and the pore traversing the length of the molecule is the single active site. Upon binding of one NADPH molecule, quenching of tryptophan fluorescence is observed. From the crystal structure, W38 is closer to bound folate than W45. Additionally, W38 is closer than W45 to NADPH docked in the active site (*17*). Thus W38 may serve as the group reporting ligand binding. To isolate the contributions of these tryptophans to the fluorescence signals monitoring pH-dependent association, dimer unfolding, and ligand binding, we have constructed single-tryptophan mutants in R67 DHFR.

MATERIALS AND METHODS

Mutagenesis. The synthetic R67 DHFR gene cloned into M13mp19 under the control of a mutant (up) promoter was used in all mutagenesis reactions (*11*). The mutagenic oligonucleotides 5′-ATTTGTGCAGTAGAACCCGACA-ATATG-3′ (W45F) and 5′-AATCTGACCTTGGAAG-GCGCC-3′ (W38F) were used to generate tryptophan → phenylalanine mutations. A Muta-Gene in vitro mutagenesis kit (Bio-Rad) was used to construct all mutations. The W38F mutant was identified by sequencing several clones; however, a low mutagenesis efficiency required that the W45F mutant be identified by dot-blot hybridization followed by sequencing. The mutant genes were then cloned into pUC8 and transformed into *Escherichia coli* (strain SK383; *18*) to increase protein expression.

Protein Purification. The mutant R67 DHFRs were expressed and purified according to Reece et al. (*11*). Briefly, bacteria were grown in a modified version of TB medium (*19*) at 37 °C to late stationary phase in the presence of 200 μg/mL ampicillin plus 50 μg/mL trimethoprim (TMP). A lower concentration of TMP, 20 μg/mL, was necessary to allow cells that contained the W38F mutant gene to grow. Cells were lysed by addition of 1 M NaOH until a pH of 12.5 was reached (*20*). Cellular debris was removed by centrifugation and the lysate was titrated to pH 2.0. Following recentrifugation, the solution was titrated to pH 6.5. Ammonium sulfate precipitation (55%) was followed by G-75 Sephadex chromatography. Further purification steps utilized DEAE-Fractogel and DEAE-Sephacel columns. A final purification step utilized a Mono-Q anion-exchange column on a Pharmacia FPLC. Purified protein was dialyzed against distilled, deionized water prior to lyophilization and storage at 4 °C. Protein concentrations were determined by the biuret method (*21*) and are expressed in terms of dimer, unless noted otherwise.

Kinetic Analysis. A Perkin-Elmer λ3a spectrophotometer interfaced with an IBM PS/2 was used to obtain steady-state kinetic data (*22*). After the addition of substrate and cofactor, the assay was initiated by addition of enzyme. The computer program UVS (Softways) allowed monitoring of initial rates by changes in absorbance at 340 nm. All assays were performed at 30 °C in a polybuffer containing 50 mM MES, 100 mM Tris, 50 mM acetic acid, and 10 mM β-mercaptoethanol (MTA buffer), pH 7.0. This buffer maintains a constant ionic strength between pH 4.5 and 9.5 (*23*). The kinetic parameters $K_{m(DHF)}$, $K_{m(NADPH)}$, and k_{cat} were determined for the W45F mutant with saturating concentrations of one substrate, either DHF or NADPH while the other was varied at subsaturating levels. The data were fit to the Michaelis-Menton equation using the nonlinear regression program, Enzfitter (Elsevier-Biosoft). Kinetic values for the W38F mutant were determined by varying both DHF and NADPH concentrations at subsaturating levels. Kinetic values were obtained as per Cleland (*24*).

Molecular Sieving Studies. To determine the apparent molecular weight of the W38F and W45F mutant proteins, gel filtration on a Superose 12 (HR 10−30) column on a Pharmacia FPLC was performed at 4 °C (12). A flow rate of 1.0 mL/min with MTA buffer, at either pH 8.0 or 5.0, was employed. Monitoring of K_{av} [= (elution volume − void volume)/(bed volume − void volume)] for protein standards (Pharmacia) allowed a standard curve to be established. The molecular weights of wt R67 DHFR (wt R67) and the W45F and W38F mutant R67 DHFRs at both pHs 5.0 and 8.0 were then calculated.

pH Dependence of Oligomeric State. To compare the pH-dependent equilibrium between tetramer and two dimers for the single-tryptophan mutants of R67 DHFR, their intrinsic protein fluorescence was monitored at room temperature as a function of pH. Previously, Nichols et al. (*12*) found a linkage between the protonation state of His62 (and its

[2] The amino acids in the first monomer are labeled 1−78; those in the second monomer, 101−178; those in the third monomer, 201−278; and those in the fourth monomer, 301−378. For brevity, when a single residue is mentioned, all four symmetry-related residues are implied.

symmetry related partners H162, H262, and H362) and a tetramer ⇌ 2 dimers equilibrium. The model proposed was

$$T \overset{K_d}{\rightleftharpoons} 2D + 2nH^+ \overset{K_a}{\rightleftharpoons} 2DH_n$$

where T is tetramer, D is dimer, DH_n is protonated dimer, K_d is a dissociation constant, and K_a is an ionization constant. This scheme can be simplified to

$$T + 2nH^+ \overset{K_{overall}}{\rightleftharpoons} 2DH_n$$

where $K_{overall}$ describes K_a^{2n}/K_d. Thus when H62 and its symmetry-related residues become protonated, they induce dissociation of tetramer. Since W38 and its symmetry-related partners also occur at the dimer−dimer interfaces, their environment can be monitored by fluorescence. An increase in solvent exposure corresponds to dissociation of tetramer.

Steady-state fluorescence measurements were performed on a Perkin-Elmer LS-5B spectrometer interfaced to an IBM PS/2 compatible computer. Tryptophan residues were excited at 295 nm and emission was monitored from 300 to 500 nm; a cell path length of 1 cm was used. For the pH titrations, the concentrations of wt R67 DHFR and the W45F mutant were held constant at 2 μM in MTA polybuffer without β-mercaptoethanol. To obtain a good signal-to-noise ratio, 16 μM W38F R67 DHFR was utilized. The samples were titrated individually with small aliquots of 2 M HCl; and pH measurements were performed directly in the cuvettes by use of a microelectrode (Microelectrodes Inc.). The intensity averaged emission wavelength, $\langle\lambda\rangle$, was monitored and plotted versus pH. $\langle\lambda\rangle$ is calculated according to

$$\langle\lambda\rangle = \sum(I_i\lambda_i)/\sum(I_i) \quad (1)$$

where I is intensity and λ is the wavelength (*10*). The intensity-averaged emission wavelength is an integral measurement and is less sensitive to noise than the change in fluorescence intensity at a fixed wavelength.

By use of the above $T + 2nH^+ \rightleftharpoons 2DH_n$ model with rate constant $K_{overall}$, the following equation can be derived:

$$F_{(obs)} = \{((F_{di} + \text{slopeA[H]}) - (F_{tet} + \text{slopeB[H]})) \times \{[H]^{2n}/(4K_{overall}P_{tot})\}\{-1 + [1 + (8K_{overall}P_{tot}/[H]^{2n})]^{1/2}\}\} + (F_{tet} + \text{slopeB[H]}) \quad (2)$$

where F_{obs} is the observed fluorescence, F_{di} and F_{tet} are the asymptotic limits for fluorescence of dimer and tetramer respectively, $K_{overall} = ([T][H]^{2n})/[DH_n]^2 = K_a^{2n}/K_d$ in units of (moles per liter)^2 for $2n = 3$, P_{tot} = the total protein concentration in terms of dimer, and slopeA and slopeB are the slopes associated with the pre- and posttransition regions, respectively (*12*). Fitting of the experimental fluorescence data to this equation utilized the NLIN subroutine in the Statistical Analysis Systems package (SAS Institute Inc., Cary, NC).

Fluorescence Quenching. Binding of NADPH to 4 μM R67 DHFR at 23 °C, pH 7, was monitored by quenching of tryptophan fluorescence as previously described (*25*). Data were fit to

$$Fl = F_0 - 0.5F_0[P_{tot} + K_d + L_{tot} - [(P_{tot} + K_d + L_{tot})^2 - 4P_{tot}L_{tot}]^{1/2}] \quad (3)$$

where Fl is the observed fluorescence, L_{tot} is the total ligand concentration, and P_{tot}, K_d, and F_0 are variables describing the number of enzyme binding sites, dissociation constant, and fluorescence yield per unit concentration of enzyme, respectively (26).

Determination of Quantum Yield. The quantum yield was determined from

$$\Phi_{prot} = \frac{\int I_{prot}\,d\lambda}{A_{prot}} \quad (4)$$

where Φ is the quantum yield, $\int I\,d\lambda$ is the integrated intensity of the emission spectrum from 300 to 450 nm, and A is the absorbance at 295 nm (*8*). Protein and tryptophan solutions had optical densities at 295 nm of ~0.03. The quantum yield of tryptophan controls was measured and normalized to 0.129 at pH 5 and 0.157 at pH 8.0 by use of the average lifetimes reported by Beddard et al. (*27*) and a quantum yield of 0.13 at pH 7 (*28*).

Equilibrium Unfolding/Folding at pH 5.0 Monitored by Steady-State Fluorescence. Tryptophan fluorescence was also used to monitor equilibrium unfolding/folding as a function of guanidine hydrochloride (GdnHCl) concentration (*11*, *25*). Changes in tryptophan fluorescence were monitored as described above with increasing concentrations of denaturant and a cell path length of 0.5 or 1 cm. Measurements were performed at room temperature (~23 °C) in MTA buffer, pH 5.0, without β-mercaptoethanol. GdnHCl concentrations were determined by refractive index measurements (*29*). The samples were incubated for >45 min to reach equilibrium. Several different concentrations of each protein were evaluated to determine the concentration dependence of the unfolding reaction.

The data for the equilibrium unfolding of R67 DHFR and the two single-Trp mutants at pH 5.0 were fit to a two-state model of unfolding, D ⇌ 2U, where D is folded dimer and U is unfolded monomer. The Gibbs free energy change, ΔG_{H_2O}, between the folded and unfolded states can then be calculated by a nonlinear fit to

$$Y_{obs} = [\{[(Y_U + M_U[\text{GdnHCl}]) - (Y_N + M_N[\text{GdnHCl}])]\,[\{\exp[-(\Delta G_{H_2O} + M_G[\text{GdnHCl}])/RT]\}^2 + 8\{\exp[-(\Delta G_{H_2O} + M_G[\text{GdnHCl}])/RT]\}[P_{tot}]]^{1/2} - \{\exp[-(\Delta G_{H_2O} + M_G[\text{GdnHCl}])/RT]\}\}/4[P_{tot}]] + Y_N + M_N[\text{GdnHCl}] \quad (5)$$

where R is the gas constant, T is the temperature, ΔG_{H_2O} is the free energy change between the native and unfolded protein in the absence of GdnHCl, M_G is the slope describing the dependence of ΔG on denaturant concentration, Y_N and Y_U are the concentration-independent optical values, and M_N and M_U are the slopes of the pre- and posttransition regions, respectively (*11*, *13*). SigmaPlot (Jandel Scientific) was used to fit the individual data sets.

To facilitate comparison between the unfolding curves, the data were normalized by use of

$$F_{app} = (Y_N - Y_{obs})/(Y_N - Y_U) \quad (6)$$

where F_{app} is the fraction of the unfolded protein, Y_{obs} is the observed value, and Y_N and Y_U are the values associated with the native and unfolded forms of the protein (*11*).

Global fits of the unfolding data using Scientist (MicroMath Scientific Software) were additionally performed to eq 5. In a global fit, all the data from a series of unfolding curves are fit concurrently to yield a single set of values. This typically results in lower errors.

Circular Dichroism. Circular dichroism (CD) spectra were recorded at 22 °C in 10 mM phosphate buffer, pH 5.0 or 8.0, for 20 μM wt R67, W45F, and W38F DHFRs. Protein concentrations were determined from the absorbance of the peptide bond according to Prasad et al. (*30*). Data were recorded from 190 to 250 nm on a Jasco J500C spectropolarimeter with a cuvette path length of 1.0 mm (*31*). For each sample, four scans were obtained at a scan rate of 5 nm/min with a time constant of 8 s; an average spectrum was then calculated. The smooth curve to the data was obtained by use of CONTIN (*32*). A buffer baseline was subtracted from the average protein scan. Data were converted to molar ellipticity (θ) by use of 108 g/mol as the mean residue molecular weight.

Time-Resolved Fluorescence. Polarized time-resolved fluorescence and decay-associated spectral (DAS) measurements were made as previously described (*33*) on a time-correlated single-photon-counting system that consists of a mode-locked Spectra-Physics (Mountain View, CA) 2045E argon-ion laser synchronously pumping a cavity-dumped Spectra-Physics model 3500 dye laser using rhodamine 6G. The latter was tuned for output at 590 nm, rotated to horizontal polarization, and then frequency-doubled for vertical emission at 295 nm by focusing into a BBO (β-barium borate) doubling crystal housed in an Inrad (Northvale, NJ) autotracker. Sample fluorescence was detected by a thermoelectrically cooled Hamamatsu (Middlesex, NJ) R3809 microchannel plate photomultiplier tube (operated at single-photon-counting voltage) after having passed through glass filters and a PRA (Oak Ridge, TN) model 1290 0.1 m monochromator. A wedge depolarizer (PRA model DPU-25) placed in front of the monochromator entrance slit was used to render the detection train polarization-insensitive (i.e., give a *G* factor of unity). Detection electronics consisted of a Hewlett-Packard (Palo Alto, CA) model 8447F fast amplifier, a Tennelec (Oak Ridge, TN) model TC454 constant fraction discriminator, and an Ortec (Oak Ridge, TN) model 457 time-to-pulse height converter. The channel width was 42 ps, and the instrument response function had a full-width at half-maximum of about 120 ps. For all measurements, the sample absorbance at the wavelength of excitation was 0.05 or less.

RESULTS

Effects of the Mutations on Steady-State Kinetics, Extinction Coefficients, and NADPH Binding. The enzymatic activities of W45F and W38F R67 DHFRs were assessed at pH 7.0 and 30 °C. Table 1 summarizes the kinetic parameters for the mutants and gives the wt values for comparison. The kinetic parameters for the W45F mutant DHFR approximate those of the wt enzyme, suggesting minimal perturbation of the active site by the mutation. In contrast, the W38F mutant R67 DHFR displays 11- and 47-fold larger K_m values for DHF and NADPH, respectively, and 100-fold smaller k_{cat} values than wt, indicating large perturbations are associated with the presence of the mutation. The W38F data were collected at a constant protein concentration of 3.3 μM dimer. Increases in the dimer concentration resulted in a greater than linear increase in activity. As indicated by molecular sieving data below, this is consistent with the W38F mutant existing predominantly as a dimer, with a very small but increasing fraction of tetramer forming in the presence of substrate.

Table 1: Comparison of Kinetic Values at pH 7.0, 30 °C

enzyme	$\epsilon_{280\ nm}$	k_{cat} (s^{-1})	$K_{m(DHF)}$ (μM)	$K_{m(NADPH)}$ (μM)
wt R67 DHFR[a]	1.87	1.3 ± 0.07	5.8 ± 0.02	3.0 ± 0.06
W45F R67 DHFR	1.29	1.3 ± 0.01	6.5 ± 0.6	4.3 ± 0.2
W38F R67 DHFR[b]	1.13	0.013 ± 0.007	65 ± 9.5	141 ± 44

[a] Values from ref *11*. [b] Values obtained with 3.3 μM dimer.

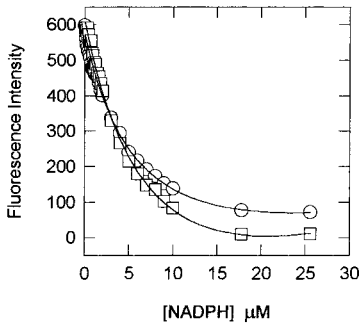

FIGURE 2: Quenching of protein fluorescence by addition of NADPH. Wild-type (4 μM) R67 DHFR (○) or W45F (4 μM) R67 DHFR (□) were each titrated with NADPH at pH 7 and the relative fluorescence intensity at 340 nm was monitored. Data were fit as described in the Materials and Methods section; best-fit values are given in the text.

Also shown in Table 1 are the extinction coefficients (ϵ_{280}) determined for each of the three proteins at 280 nm, pH 8. The ϵ_{280} values for the two single-tryptophan mutants are significantly lower than for wt R67 DHFR, consistent with loss of one tryptophan per monomer.

The binding of NADPH to wt and W45F R67 DHFRs was also monitored by fluorescence quenching as shown in Figure 2. For wt R67 DHFR, best fits yielded a K_d of 5.3 ± 0.57 μM with $n = 0.67 \pm 0.05$; for W45F R67 DHFR, $K_d = 6.7 \pm 0.86$ μM and $n = 0.91 \pm 0.098$. These results indicate similar binding of NADPH to both wt and W45F R67 DHFRs. The extent of fluorescence quenching is similar in both proteins (87% vs 98% for wt and W45F, respectively), indicating that perturbations in the environment of W38 monitor NADPH binding, consistent with the closer proximity of W38 to bound ligands than W45. NADPH binding to W38F R67 DHFR was not examined as its K_m was so high.

Gel-Filtration Studies. Molecular sieving chromatography was utilized to assess the oligomeric state of the mutant R67 DHFRs since W38, W138, W238, and W338 occur at the dimer−dimer interfaces while W45, W145, W245, and W345 occur at the monomer−monomer interfaces. These mutations might alter the association state of R67 DHFR. Table 2 summarizes the apparent molecular weights determined for wt, W45F, and W38F R67 DHFRs at pH 5 and 8.

Table 2: Molecular Sieve Data at pH 5.0 and 8.0

	K_{av}	calculated MW
	pH 5.0	
wt R67 DHFR	0.549	26 700 ± 70
W38F R67 DHFR	0.530	28 900 ± 150
W45F R67 DHFR	0.543	27 500 ± 700
	pH 8.0	
wt R67 DHFR	0.382	49 000 ± 650
W38F R67 DHFR	0.514	25 000 ± 640
W45F R67 DHFR	0.407	43 500 ± 1400

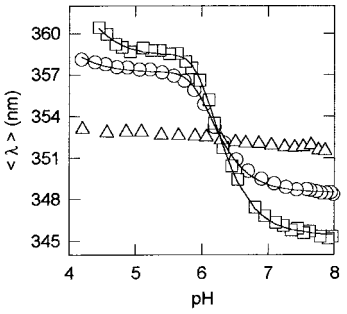

FIGURE 3: pH titration of R67 DHFRs monitored by fluorescence. The intensity averaged wavelength, $\langle\lambda\rangle$, for wt (○), W45F (□) and W38F (△) R67 DHFRs was monitored as a function of pH. The protein concentration of wt and W45F R67 DHFRs was 2 μM, while that of the W38F mutant was 16 μM. The W45F and wt R67 DHFR data were each fit to eq 2, and best-fit values are listed in Table 3.

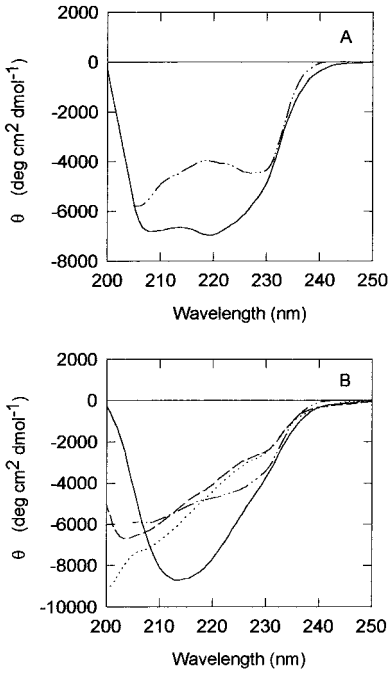

FIGURE 4: Assessment of secondary structure in R67 DHFR by CD. Panel A displays the scans of the various tetrameric species: wt R67 DHFR at pH 8 (—) and W45F R67 DHFR at pH 8 (—••—). Panel B displays the scans of the various dimeric species: wt R67 DHFR at pH 5 (—), W45F R67 DHFR at pH 5 (—••—), W38F R67 DHFR at pH 5 (•••), and W38F R67 DHFR at pH 8 (— — —). Data are presented as the mean residue ellipticity, θ, by taking 108 g/mol as the mean residue molecular weight.

At pH 5.0, the two mutant R67 DHFRs have apparent molecular weights that are similar to wt values. Since wt R67 DHFR is dimeric at pH 5.0 (*12*), this result is consistent with W38F and W45F R67 DHFRs also being dimeric at pH 5.0. At pH 8.0, the K_{av} shifts for both the wt and the W45F mutant proteins, consistent with tetramer formation. In contrast, the K_{av} for W38F R67 DHFR stays constant, consistent with it remaining dimeric at pH 8.0. Clearly stacking of W38−W338 (and W138−W238) at the dimer−dimer interfaces is important in tetramer stability, and the presence of four simultaneous W38F mutations at these two interfaces is sufficient to preclude tetramer formation.

pH Dependence of the Oligomeric State. The oligomeric state of the mutant proteins was further characterized by monitoring fluorescence as a function of pH. Figure 3 shows the change in intensity averaged emission wavelength, $\langle\lambda\rangle$, as a function of pH. A transition for both the wt and W45F mutant R67 DHFRs is observed, consistent with dissociation of tetramer to 2 dimers as the pH is decreased from 8.0 to 5.0. The red shift in $\langle\lambda\rangle$ as the pH is decreased corresponds with exposure of W38 to solvent. In striking contrast, the W38F mutant R67 DHFR displays only a linear increase in $\langle\lambda\rangle$, consistent with the destabilization of the tetramer and minor pH effects on the environment of W45 in the dimer.

The experimental data for wt and W45F R67 DHFRs were fit to eq 2 and best-fit values (for $2n = 3$) are given in Table 3. $2n$ corresponds to the number of protons acquired by the symmetry-related His 62 residues at the dimer−dimer interfaces. The pH titration data for wt and W45F R67 DHFRs yielded $K_{overall}$ values that are in agreement within experimental error, indicating the W45F mutation does not affect the dependency of the oligomeric state on the pH. This observation is consistent with W45 being distant from the dimer−dimer interfaces.

Circular Dichroism Scans, pH 8.0. To assess the effects of the W45F and W38F mutations on the secondary structure of R67 DHFR, CD spectra for equivalent concentrations of wt, W45F, and W38F R67 DHFRs are shown in Figure 4. Significant differences in the CD scans of the three proteins are seen at both pHs 8 and 5. These differences could be due to structural alterations that accompany the mutations. Alternatively, Woody (*34*) indicates aromatic side chains can make detectable contributions to the far-UV CD. The loss of tryptophan could directly diminish the CD signals. This model appears possible as mathematical addition of the W38F and W45F signals at pH 5 yields a trace that is very similar to that of wt R67 DHFR from ∼218 to 250 nm (not shown).

Alterations in Fluorescence Emission Spectra and Relative Quantum Yields at pH 5.0 and 8.0. The effects of the W45F and W38F single-tryptophan mutations on fluorescence in R67 DHFR were determined as shown in Figure 5. At equivalent protein concentrations, both mutants show a decrease in fluorescence intensity, consistent with the loss

Table 3: Best-Fit Values for the pH-Dependent Dissociation of Tetramer ⇌ 2 Dimers

enzyme	$K_{overall}$ (M^2)	limit1 (nm)	limit2 (nm)	slopeB	slopeA
wt R67 DHFR	$1.42 (\pm 0.85) \times 10^{-13}$	357 ± 0.1	348 ± 0.1	18.3 ± 3.9	2890 ± 1830
W45F R67 DHFR	$1.50 (\pm 0.50) \times 10^{-13}$	358 ± 0.2	345 ± 0.1	62.5 ± 7.4	6650 ± 1340

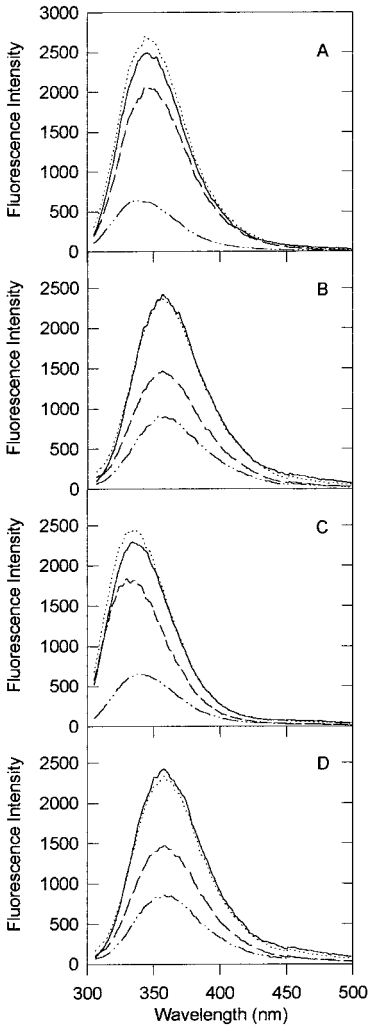

FIGURE 5: Comparison of fluorescence emission spectra. Panel A shows the scans for the three proteins in buffer at pH 5, and panel B shows their spectra in 4 M GdnHCl at pH 5. Panels C and D show the three proteins at pH 8 in buffer and 4 M GdnHCl, respectively. (—) Wt R67 DHFR data; (– – –) W45F data; (—••—) W38F R67 DHFR scans. Mathematical addition of the W38F and W45F scans is shown by the dotted lines (•••).

of a tryptophan from the structure. However, the effect on intensity is much more dramatic in the W38F mutant as compared to the W45F mutant, suggesting W38 contributes more to the total fluorescence signal than W45. Recall that the W45F mutant R67 DHFR contains only W38, while the W38F mutant contains only W45.

At pH 5.0, the W38F R67 DHFR scan is blue-shifted compared to the wt or W45F R67 DHFR scans. This result is consistent with sequestering of W45 (in the W38F mutant) at the monomer−monomer interface, whereas W38 is exposed in dimeric wt and W45F R67 DHFRs. When the W45F and W38F R67 DHFR scans are added, they generate a scan similar to that of wt R67 DHFR (dotted line), suggesting the effects of the mutations on fluorescence intensity are mostly additive in the native dimeric structure. In 4 M GdnHCl at pH 5, the emission intensity scans of the W38F and W45F mutants are again lower than wt and the addition of their scans yields a curve within error of wt. This latter result indicates the fluorescence of mutant proteins is additive under denaturing conditions.

Table 4: Quantum Yields for the Various R67 DHFRs

	quantum yield (Φ)	λ_{max} (nm)
	pH 5.0	
wt R67 DHFR	0.12	346
W38F R67 DHFR	0.055	341
W45F R67 DHFR	0.13	346
	pH 8.0	
wt R67 DHFR	0.12	338
W38F R67 DHFR	0.065	342
W45F R67 DHFR	0.21	330

At pH 8.0, the fluorescence intensity scans for both mutants are again observed to be less than wt, with a greater intensity for the W45F R67 DHFR as compared to W38F. Additionally, the scan for W45F R67 DHFR is more blue-shifted than that of the W38F mutant. This is consistent with W38 being buried in tetrameric W45F R67 DHFR at pH 8.0 and exposed in dimeric R67 DHFR. Since the W38F mutant remains dimeric at pH 8, a comparison of $\langle\lambda\rangle$ for the W38F and W45F mutants may be taken to indicate which Trp is more buried. Since $\langle\lambda\rangle$ is lower for the W45F mutant (with W38 buried at the dimer−dimer interfaces) than for the W38F mutant (with W45 buried at the monomer−monomer interfaces), this suggests that W38 is more buried than W45 in tetrameric R67 DHFR (see Figure 3). This observation also corresponds with the solvent-accessible surface area calculated with Insight (Molecular Simulations, San Diego, CA) with a probe radius of 1.4 Å. For W38 in dimeric R67 DHFR, this value is ~42 Å^2, which shrinks to ~7 Å^2 in the tetramer. For W45 at both pHs, the solvent-accessible area is ~81 Å^2. Finally, in 4 M GdnHCl at pH 8, when the scans for the mutants are added, they generate a scan almost identical with that of wt, indicating additive effects under denaturing conditions.

The quantum yields for the various R67 DHFRs were additionally calculated and are given in Table 4 as well as the λ_{max}. The quantum yields for W38F and W45F R67 DHFRs are lower and higher than the wt value, respectively. However, the extinction coefficient-weighted average quantum yield calculated for the sum of the W38F and W45F R67 DHFRs is practically identical to that of wt R67 DHFR at pH 5.0, indicating the mutations do not alter the dimer conformation. Eftink (*35*) has listed the quantum yield values for several single-Trp mutants and notes a large range compared to a control Trp value of 0.13. For example, Φ values for phosphofructokinase, ribonuclease T_1, melittin, and phospholipase A_2 are 0.35, 0.31, 0.115, and 0.031, respectively.

Equilibrium Unfolding Studies. To investigate the effects of these mutations on the structural stability of R67 DHFR, equilibrium unfolding studies at pH 5.0 were performed at increasing concentrations of GdnHCl. Figure 6A shows the equilibrium unfolding transitions for 1 and 4 μM W45F R67 DHFR monitored by changes in fluorescence intensity at 340 nm. A clear dependence on the concentration of protein is seen, as predicted from the bimolecular nature of the dimer $\rightleftharpoons$ 2 unfolded monomers reaction. The data for each protein concentration were fit individually to a two-state unfolding model, and best-fit values are summarized in Table 5. In addition, four data sets were fit globally to obtain a single ΔG_{H_2O} value with lower error (2.5 and 10 μM data sets were

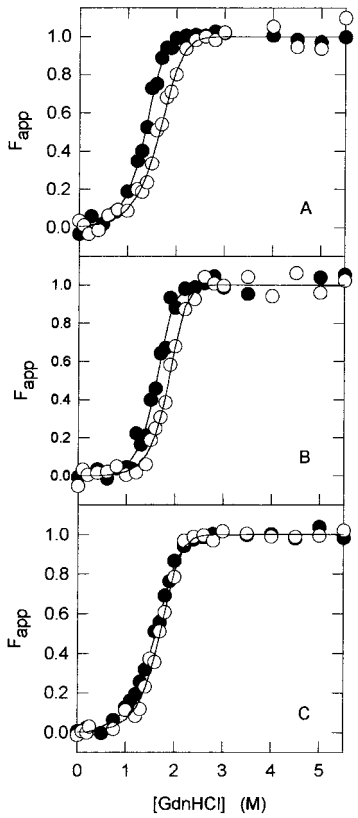

FIGURE 6: Equilibrium unfolding/folding of W45F and W38F R67 DHFRs at pH 5.0. The fluorescence intensity at 340 nm for R67 DHFR was monitored as a function of GdnHCl concentration and plotted. Panel A shows W45F R67 DHFR data collected at 1 (●) and 4 μM (○). Panel B shows W38F R67 DHFR data collected at 1 (●) and 4 μM (○). The data sets were fit individually and best-fit values are given in Table 5. The data were also fit globally; best-fit values are given in Table 6. For comparison, wt R67 DHFR data at 1 (●) and 4 μM (○) are shown in panel C.

Table 5: Best Fits of Equilibrium Unfolding/Folding Data at pH 5.0

condition	ΔG_{H_2O} (Kcal/mol)	M_G (kcal mol^{-1} M^{-1})
wt R67 DHFR (1 μM)	12.4 ± 0.2	−3.4 ± 0.2
wt R67 DHFR (4 μM)	13.7 ± 1.1	−3.9 ± 0.6
W45F R67 DHFR (1 μM)	13.6 ± 0.4	−4.3 ± 0.3
W45F R67 DHFR (4 μM)	12.7 ± 1.1	−3.5 ± 0.6
W38F R67 DHFR (1 μM)	15.3 ± 1.5	−4.7 ± 0.8
W38F R67 DHFR (4 μM)	15.6 ± 1.3	−4.6 ± 0.6

Table 6: Global-Fit Values for Equilibrium Unfolding/Folding Data at pH 5.0

enzyme	ΔG_{H_2O} (kcal mol^{-1})	M_G (kcal mol^{-1} M^{-1})
wt R67 DHFR[a]	13.2 ± 0.2	−3.8 ± 0.1
W45F R67 DHFR[b]	12.4 ± 0.2	−3.4 ± 0.1
W38F R67 DHFR[c]	14.9 ± 1.0	−4.6 ± 0.6

[a] Includes 1, 4, 6, and 10 μM dimer data sets. [b] Includes 1, 2.5, 4, and 10 μM dimer data sets. [c] Includes 1, 4, and 10 μM dimer data sets.

not shown in Figure 6 for clarity). These fit values are given in Table 6.

Figure 6B shows the equilibrium unfolding transitions of 1 and 4 μM W38F R67 DHFR. A protein concentration dependence is again observed. The best-fit values for each individual data set are given in Table 5. Three data sets were fit globally (including a 10 μM data set, not shown in Figure 6); these fit values are given in Table 6.

Figure 6C shows the equilibrium unfolding transitions of 1 and 4 μM wt R67 DHFR. The best-fit values for each individual data set are again given in Table 5 and the global-fit values for three data sets (10 μM data set not shown in Figure 6) are given in Table 6.

Time-Resolved Fluorescence Measurements. The native wt and mutant proteins were further characterized by time-resolved fluorescence and the results are listed in Table 7 and shown in Figure 7. A sum of three exponentials with τ values of about 0.7, 2, and 5 ns gave the best fits for the wt and W38F mutant proteins at both pH 5 and 8. In contrast, the fluorescence decays of the W45F mutant at these two pHs were adequately described by just two exponentials, with lifetimes of approximately 2 and 5 ns. (The fluorescence decay of the W45F mutant at pH 5 is almost completely monoexponential.) In the case of the wt and W45F mutant proteins, the fractional contributions each component makes to both the decay amplitude (c_i in Table 7) and steady-state fluorescence intensity (as shown by the intensity DAS in Figure 7) change greatly upon dimer-to-tetramer association. In the wt and W45F mutant dimers at pH 5, the 5 ns component dominates the fluorescence decay and steady-state fluorescence intensities, whereas the 2 ns component is the major one in the respective tetramers at pH 8. Most likely this difference is due to the change in the environment of the W38 residues at the dimer−dimer interface as they become less exposed to the solvent (and come into closer proximity with one another) upon forming tetramers. In the case of the W38F mutant, the relative contributions of the individual decay components change little upon going from pH 5 to pH 8. This is consistent with our molecular sieving results, which indicate this mutant remains a dimer at pH 8. (In any case, dimer-to-tetramer association would not be expected to affect the environment of the W45 residues located at the monomer−monomer interface.)

Except for the wt and W45F tetramers at pH 8, a single exponential was found to adequately describe the fluorescence anisotropy decay in each case, and the rotational correlation times (ϕ) are consistent with the expected molecular weights of the respective species (Table 7). (A globular protein of about the same molecular weight as the wt dimer (~16 kDa) would be expected to have a ϕ of ~8 ns.) This suggests that in almost all cases the fluorophore motion is dominated by the overall tumbling of the protein. The ϕ values are consistent with the expected states of oligomerization based on the molecular sieve results and confirm that the W38F mutant remains dimeric at pH 8. In the case of the wt protein at pH 8, there also appears to be a subnanosecond component ($\phi \approx 0.7$ ns, Table 7) in the anisotropy decay that may arise from either local side-chain motion or some fast electronic depolarization process. (The former explanation seems unlikely, however, as no such local motion was detected in the dimeric form of the protein, and the dimer-to-tetramer association might be expected to restrict further the motion of the W38 indole side chain rather than to make it more mobile.) Although a double exponential best described the anisotropy decay of the W45F mutant at pH 8, the parameters' confidence limits were sufficiently broad that the results of a single-exponential analysis are reported instead (Table 7). In all cases, the initial anisotropy values ($r_0 = \Sigma_i \beta_i$) are significantly lower than what is typically observed in time-resolved anisotropy measurements of tryp-

Table 7: Time-Resolved Fluorescence Intensity and Anisotropy Decay Parameters of Native wt, W38F, and W45F R67 DHFR (λ_{em} = 335 nm)[a]

WT, pH 5		W38F, pH 5		W45F, pH 5	
c_i (± SD)	τ_i (± SD) (ns)[b]	c_i (± SD)	τ_i (± SD) (ns)	c_i (± SD)	τ_i (± SD) (ns)
0.301 (±0.095)	0.62 (±0.08)	0.453 (±0.044)	0.72 (±0.03)	0.156 (±0.071)	1.36 (±0.16)
0.321 (±0.062)	1.95 (±0.25)	0.504 (±0.030)	1.96 (±0.06)	0.843 (±0.071)	5.21 (±0.03)
0.378 (±0.041)	5.28 (±0.12)	0.043 (±0.005)	5.38 (±0.30)		
β = 0.117 (±0.015)		β = 0.100 (±0.008)		β = 0.140 (±0.004)	
ϕ = 10.8 (±0.9) ns		ϕ = 7.9 (±1.0) ns		ϕ = 7.8 (±0.6) ns	
WT, pH 8		**W38F, pH 8**		**W45F, pH 8**	
c_i (± SD)	τ_i (± SD) (ns)	c_i (± SD)	τ_i (± SD) (ns)	c_i (± SD)	τ_i (± SD) (ns)
0.298 (±0.067)	0.75 (±0.08)	0.421 (±0.045)	0.66 (±0.03)	0.888 (±0.042)	2.46 (±0.03)
0.642 (±0.074)	2.23 (±0.06)	0.507 (±0.032)	1.87 (±0.07)	0.112 (±0.042)	5.42 (±0.27)
0.060 (±0.008)	5.17 (±0.33)	0.072 (±0.007)	4.84 (±0.23)		
β_1 = 0.023 (±0.008)	ϕ_1 = 0.66 (±0.37) ns	β = 0.088 (±0.017)		β = 0.071 (±0.017)	
β_2 = 0.088 (±0.016)	ϕ_2 = 15.4 (±4.1) ns	ϕ = 8.4 (±1.6) ns		ϕ = 15.9 (±3.1) ns	

[a] A minimum of two independent measurements was made on the wt and two mutant enzymes for the two different pH values reported. The lifetimes τ_i and fractional amplitudes $c_i = \alpha_i/\Sigma_j\alpha_j$ listed come from the DAS analyses rather than the polarized fluorescence decay data, as a global analysis of fluorescence decay data obtained for a range of emission wavelengths generally yields more accurate parameter values than does an analysis of decay data acquired at a single emission wavelength (*48*). DAS measurements also are preferred, as fluorescence decay data collected over a broad range of emission wavelengths should reveal the presence of decay components that might otherwise be missed in data collected at just a single emission wavelength. For all our data, however, the fluorescence lifetimes and fractional amplitudes obtained from the polarized fluorescence decay data were in good agreement with their corresponding values from the DAS analyses. The accuracy of the fluorescence intensity decay parameters listed in the table was further improved by obtaining them from a simultaneous analysis of several (typically three) separate DAS data sets acquired for the same sample conditions. The decay times listed in the table are those that resulted from the simultaneous analyses and their uncertainties were calculated directly from the lifetimes' 68% confidence limits. In the case of the fractional amplitudes (c_i) at the peak emission wavelength, their stated values are the averages of the values obtained for each of the data sets included in the simultaneous analysis. Their uncertainties were determined either from the variation between the individual c_i, or from their 68% confidence limits, whichever gave the larger number. The results of the simultaneous analyses were nevertheless in good agreement with the averages of the parameter values obtained from the separate analyses of the same individual data sets. [b] A fourth decay component with lifetime fixed at 20 ps was used in fitting to model any background that did not subtract out with the baselines.

tophan fluorescence in proteins ($r_0 \approx 0.2$). This suggests that some fast depolarization process is at work that is beyond the temporal resolution of the picosecond fluorometer that was used (see Discussion). The value for β observed for the W45F mutant at pH 5 is somewhat higher than that obtained for the wt and W38F mutant proteins, however, which suggests that whatever fast depolarization process is at work for the latter two cases has less of an effect in the W45F dimer. Fluorescence resonance energy transfer (FRET) as a possible candidate for this process would certainly be less likely in this case as the two remaining tryptophan residues (W38 and W138, located at opposite ends of the dimer−dimer interface) are separated by a much greater distance (~18 Å) than are the W38 and W338 residues that face each other in the tetramer at pH 8, for which β has decreased by about half. (The CZ3 (C5) atoms of W38 and W238 residues are in van der Waals contact in that case.)

DISCUSSION

Effects of the W45F Mutation. Numerous experiments indicate the W45F mutation does not substantially alter either the structure or catalytic function of R67 DHFR. First, the k_{cat} and K_m values for wt and W45F R67 DHFRs are similar at pH 7.0 (Table 1). Second, binding of NADPH monitored by fluorescence quenching yields similar K_d values for wt and W45F R67 DHFR. Third, the W45F mutant undergoes a tetramer to 2 dimers transition as a function of pH when monitored by molecular sieving and fluorescence techniques. The $K_{overall}$ values describing the pH-dependent dissociation of tetramer are in agreement for wt and W45F R67 DHFRs (Table 3). Last, the ΔG_{H_2O} values describing equilibrium unfolding of the dimer indicate wt R67 DHFR is only slightly more stable than W45F R67 DHFR (see global-fit values in Table 6). These results all suggest the W45F mutation does not significantly affect either the oligomeric structure or the catalytic function of R67 DHFR.

Effects of the W38F Mutation. In contrast, the W38F mutation appears to have significantly affected the oligomeric state and thus the function of R67 DHFR. Since the W38F mutation occurs at the dimer−dimer interface, the cumulative effect of four mutations is to destabilize the tetramer. This results in a decreased ability of the W38F R67 DHFR gene to confer TMP resistance upon host *E. coli*. Also, the molecular sieving and pH-dependent fluorescence data as well as the time-resolved fluorescence anisotropy measurements conclusively show the W38F mutant remains dimeric throughout the pH range 5−8. Finally, a large decrease in catalytic efficiency is observed since the active-site pore is no longer present in dimeric W38F R67 DHFR. The only suggestion of tetramer formation occurs in the steady-state kinetic data, as a nonlinear protein concentration dependence is observed, suggesting a low level of tetramer may form in the presence of substrate.

The above results lead us to an alternate question: does the W38F mutation alter the structure and function of dimeric R67 DHFR? Decreased enzyme activity has previously been observed in R67 DHFRs that were either modified or engineered to remain in the dimeric form. Wt R67 DHFR treated with diethyl pyrocarbonate (DEPC), a reagent that modifies histidine residues by adding a bulky *N*-carbethoxy group, disrupts the dimer−dimer interface by modifying His 62 (*12*). The DEPC-treated wt R67 DHFR dimers displayed

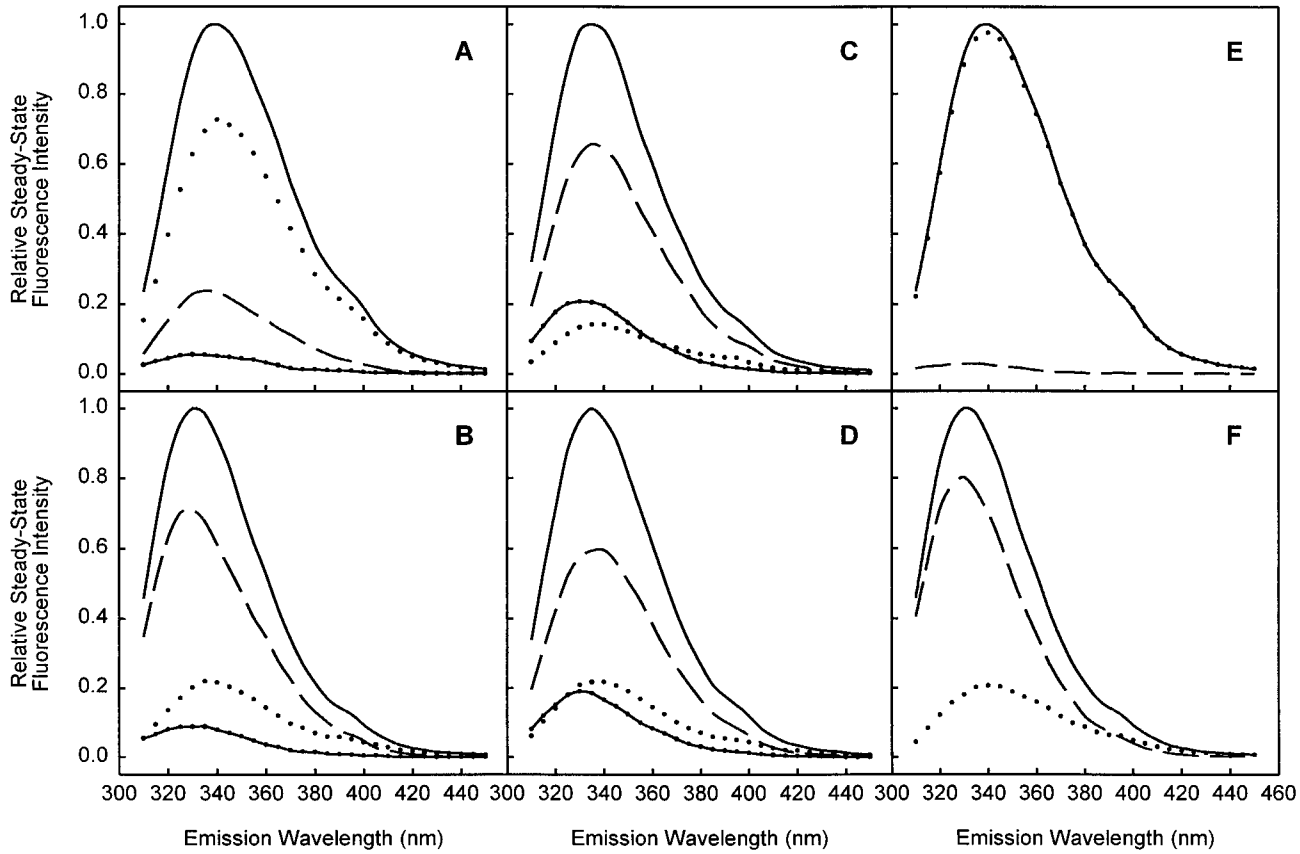

FIGURE 7: Plots of the steady-state fluorescence intensity vs emission wavelength ("intensity DAS") for the fluorescence decay components observed in native wt (panels A and B), W38F (panels C and D), and W45F (panels E and F) R67 DHFR. For each species, the upper panel shows the spectra at pH 5 while the lower panel shows them for pH 8. In each panel, the solid line with dots (where present) shows the contribution the subnanosecond component makes to the spectrum, while the dashed and dotted lines show those of the intermediate ($\tau \approx$ 2 ns) and long ($\tau \approx 5$ ns) components, respectively. Their sum, which gives the total steady-state fluorescence spectrum, is shown by the solid line. The DAS were obtained by measuring the sample's total fluorescence intensity decay (with the emission polarizer set at the magic angle) at 5 nm intervals over the wavelength range of 310−455 nm, according to Green et al. (*33*). The data were globally analyzed with the constraint that the same fluorescence decay times be used in fitting the data from all the emission wavelengths using in-house deconvolution software, according to Knutson et al. (*48*). The sum of the $\alpha_i(\lambda)\tau_i$ products was normalized to the sample's steady-state emission spectrum [obtained with an SLM 8000 spectrofluorometer (Urbana, IL) operated in single-photon counting mode and with the spectrum rescaled to unit peak intensity] according to eq 5 of Kim et al. (*49*) to obtain the fractional steady-state fluorescence intensity of the *i*th decay component at the emission wavelength λ. Note: The long-wavelength shoulder centered at about 400 nm is most likely due to the so-called Wood's anomaly sometimes observed in the output of monochromators.

a $K_{m(DHF)}$ of 40 ± 4.0 μM, a $K_{m(NADPH)}$ of 72 ± 5.5, and a k_{cat} of 0.052 ± 0.007 s^{-1}. Additionally, a dimeric H62C mutant R67 DHFR (reducing conditions) displayed $K_{m(DHF)}$ = 36 ± 4.0 μM, $K_{m(NADPH)}$ of 74 ± 6, and a k_{cat} of 0.033 ± 0.002 s^{-1} (*36*). The similarity of the kinetic values for these dimeric R67 DHFRs with the W38F mutant suggests the W38F mutation has not greatly perturbed the catalytic activity of the dimer. Finally, the ΔG_{H_2O} values describing equilibrium unfolding of the dimer indicate wt R67 DHFR is only slightly less stable than W38F R67 DHFR (Table 6). These results indicate the function of dimeric R67 DHFR is not greatly compromised by the presence of the W38F mutations. Thus the main effect of the W38F mutation from these studies appears to be destabilization of the tetramer.

Effects on Protein Stability. From the equilibrium unfolding/folding data, small differences in protein stability are observed. The ΔG_{H_2O} values obtained by global fitting of several unfolding curves indicate W38F R67 DHFR is slightly more stable than the wt protein, which in turn is slightly more stable than the W45F mutant. Since W45 is partially buried at the monomer−monomer interface and stacks with its symmetry-related partner, W145, substitution of this residue by phenylalanine may affect packing and thus stability. That the W38F mutant is slightly more stable is surprising as W38 occurs on the surface of the dimer and introduction of a more hydrophobic residue might be expected to be destabilizing (*37*−*39*). Alternately, the environment of W38 is monitored by the W45F mutant and since W38 is exposed, it might be envisioned to unfold prior to unfolding of the hydrophobic dimer core. The latter may be monitored by W45 in the W38F mutant. Thus the two mutants may be monitoring different environments that unfold at slightly different denaturant concentrations.

Relative Contributions of W38 and W45 to R67 DHFR Fluorescence. From the fluorescence emission curves of W38F and W45F R67 DHFRs (Figure 5) as well as the quantum yield values, it is clear that the overall contribution of W38 to R67 DHFR fluorescence is much greater than that of W45. From this observation alone, it would be likely that its signal would be more dominant in the processes measured by fluorescence, e.g., pH titration of fluorescence and fluorescence quenching upon addition of NADPH. In addition, the position of W38 at the dimer-dimer interface makes it the prime candidate for monitoring the pH-

dependent dissociation of tetramer. Also, the proximity of W38 to bound folate and docked NADPH in the crystal structure (*17*) suggested it would be the primary fluorophore. The two mutants described in this report have enabled us to sort out the relative contributions of W38 and W45 to fluorescence of R67 DHFR and corroborate our predictions from analysis of the crystal structure. In addition, the presence of only two tryptophans per monomer has facilitated our analysis as fluorescence complexity in R67 DHFR mostly arises from the D_2 symmetry that amplifies the effect of a single mutation on the gene level to two (or four) simultaneous mutations per dimer (or tetramer).

Since only the W38 environment is monitored in the W45F mutant, the pH dependence of fluorescence clearly shows that W38 is the fluorophore that monitors the pH-dependent dissociation of tetramer to 2 dimers (Figure 3). Only a linear increase in fluorescence is noted as the W38F mutant is titrated from pH 8 to 5, consistent with titrations in dimeric R67 DHFR affecting the fluorescence of W45 to a minor degree.

Further, W38 can also be designated as the fluorophore monitoring the binding of NADPH to R67 DHFR (Figure 2). While the effect of W45 on these process was not measured directly (since W38F R67 DHFR is dimeric and the K_d for NADPH was high and out of the linear range of the fluorometer), its contribution appears minimal. This is deduced from the percent (fluorescence) quench observed upon NADPH addition to wt and W45F R67 DHFRs, which is 87% and 98%, respectively. This 11% quench difference is likely to be due to the baseline contribution of W45 to the overall fluorescence; thus complete quenching of protein fluorescence does not occur in wt R67 DHFR.

From these results, the fluorescence signal is clearly dominated by W38. Differences in the local environments of W38 versus W45 as well as the degree of solvent exposure are likely to influence their contributions to the fluorescence signal (*40*).

Do the Mutant Spectra Show Additivity? The time-resolved fluorescence decay measurements indicate that the mutant spectra are "additive" and sum to yield the wt spectrum for the following reasons:

(i) There is good agreement between the fluorescence decay times obtained for the mutant and wt proteins. This suggests that mutation to Phe of either of the Trp residues has little or no effect on the fluorescence properties of the remaining Trp. In this regard, it should be noted that a simultaneous analysis of three DAS data sets, one each for the native wt, W38F, and W45F enzymes at pH 5, gave excellent fits for which the residuals and autocorrelation function values were random and the global χ_R^2 value was unity. Also, the resulting lifetimes and fractional decay amplitudes were in excellent agreement with those obtained from the separate analyses of the individual data sets. The simultaneous analysis yielded best-fit lifetime values of 0.72, 1.95, and 5.25 ns. In this case, the decay of the W45F mutant was again virtually monoexponential (with $\tau = 5.25$ ns as before), while the subnanosecond component again made a relatively large contribution (~21% at the peak wavelength) to the steady-state intensity of the W38F mutant.

(ii) The time-resolved results are consistent with the conclusion that, at pH 5, W38 contributes almost all of the 5 ns decay component of the wt enzyme, while W45 provides most of the enzyme's subnanosecond and 2 ns decay components. This follows from the fact that the 5 ns component makes only a minor contribution to the decay of W38F, while the W45F mutant has no subnanosecond component and only a minor contribution from an ~2 ns component. Further, the ratio of the steady-state fluorescence intensities for the 2 ns and ~0.7 ns components is the same (about 3:1) in both wt and the W38F mutant at pH 5. Given these lifetime assignments and the decay components' relative steady-state intensities in the wt enzyme (see Figure 7A), it would then be expected that the W45F and W38F mutants would have a quantum yield ratio of about 2:1, which is consistent with the quantum yields reported in Table 4. (This argument assumes that the extinction coefficients of the two Trp residues are the same, and it can be seen from Table 1 that they are close.)

From the data in Table 7, it is clear that W45 is also responsible for all the subnanosecond fluorescence decay observed in the wt enzyme at pH 8. (Most of the remaining steady-state fluorescence intensity results from the 2 ns lifetime decay.) An analysis of the pH 8 data similar to that carried out in the preceding paragraph indicates that in this case the quantum yields of W38F and W45F mutants should again differ by about a factor of 2. This conclusion is fairly consistent with the results shown in Table 3 and indicates that the mutant spectra are additive at pH 8 as well. A simultaneous analysis of wt, W38F, and W45F DAS data at pH 8 gave results that were also in good agreement with the values listed in Tables 7, which further reinforces the judgment about their additivity. (The lifetime values from the simultaneous analysis were 0.86, 2.30, and 5.10 ns.)

What Produces the Low Initial Anisotropy Values? The initial anisotropy values ($r_0 = \Sigma\beta_i$) obtained from the time-resolved measurements are significantly lower than values typically observed for Trp fluorescence in proteins. [$r_0 \approx$ 0.25 and 0.20 for the single Trp residues in horse heart apocytochrome *c* (*41*) and adrenocorticotropin (*42*), respectively, and ~0.2 for horse liver alcohol dehydrogenase (the latter with two Trp residues; *43*)]. This suggests that some fast initial depolarization process is at work that is beyond the resolution of the picosecond time-resolved fluorometer that was used. In general terms, fluorescence resonance energy transfer (FRET), excited-state proton transfer between chromophore molecules, and excimer formation are all photophysical processes that are known to cause fluorescence depolarization. Such excited-state processes usually result, however, in the presence of a negative long-wavelength component in the DAS (*44*, *45*) that was not observed here. With regard to FRET, however, the absence of such a negative term could be due to the fact that the symmetry-related tryptophan residues in R67 DHFR that could be interacting are completely interchangeable, so that emission from either of two such Trps would have to be identical to emission from the other. In other words, any photons lost by the "donor" in such a process would have to be re-emitted unchanged by the "acceptor." Also, Eftink et al. (*46*) have shown, using simulations of phase-resolved spectra (PRS, the phase-modulation analogue of DAS) for two-Trp proteins in the presence of FRET, that a negative component may not be observed in the PRS if the emission peaks of the two Trps are not widely separated. Thus, the absence of a negative DAS term need not rule out FRET as contributing

to the fluorescence depolarization. Future measurements with a femtosecond fluorescence upconversion system may enable us to better resolve the initial anisotropy values and fluorescence decay kinetics for these proteins.

In considering the possibility of Trp−Trp excimer formation, it should be noted that the initial anisotropy r_0 of the W45F mutant drops by about half upon dimer-to-tetramer association. The latter process should, however, further restrict the motion of the W38 indole side chain and so increase its fluorescence anisotropy rather than decrease it. Upon tetramer formation, the CZ3 (C5) atom of the W38 indole ring comes into van der Waals contact with the CZ3 (C5) and CH2 (C6) atoms of the (now) adjacent W338 indole ring. The side chain of H262 further "fills in" the space surrounding the W38 side chain so that the latter's solvent-accessible surface area is reduced. Given the inter-Trp distances involved, however, and the relative orientations and restricted mobilities of their respective side chains, W38−W338 excimer formation probably does not play a significant role in the excited-state interactions of R67 DHFR. W45−W145 excimer formation would also seem to be unlikely because of their inter-Trp distances and relative orientations. In any case, excimer emission is typically at longer wavelengths with respect to that of the monomer; the symmetry argument made in the case of FRET would not apply here, and excimer emission should be observable if it were taking place. Excited-state proton transfer is not anticipated to play a role either, as any nearby aromatic residues should already be protonated and would not serve as proton acceptors. This leaves FRET as being the most likely cause of the initial fluorescence depolarization observed in the native proteins.

To conclude, our predictions concerning the contributions of W38 and W45 to ligand binding, pH effects, and dimer unfolding in R67 DHFR as monitored by fluorescence (based on analysis of the crystal structure) are supported by the results presented in this paper. In addition, our results suggest the role played by W45 in maintaining the monomer−monomer interface is less crucial than the role played by W38 in maintaining the dimer−dimer interface. This comment arises as substitution of Phe (135 Å^3 van der Waals volume; *49*) for Trp (163 Å^3) at W38 greatly destabilizes tetramer, while the analogous substitution at W45 only slightly destabilizes dimer.

ACKNOWLEDGMENT

We thank Dr. Peter McPhie (NIDDK, NIH) for his assistance in making the CD measurements. T.D.B. thanks the Optical Spectroscopy Section (OSS), National Heart, Lung and Blood Institute (NHLBI), NIH, for the use of its facilities. The helpful discussions of Dr. Jay R. Knutson, Chief, OSS, NHLBI, NIH, are also gratefully acknowledged.

REFERENCES

1. Eftink, M. R. (1994) *Biophys. J. 66,* 482−501.
2. Helms, M. K., Hazlett, T. L., Mizuguchi, H., Hasemann, C. A., Uyeda, K., and Jameson, D. M. (1998) *Biochemistry 37,* 14057−14064.
3. Dijkstra, S. D., Broos, J., Visser, A. J. W. G., van Hock, A., and Robillard, G. T. (1997) *Biochemistry 36,* 4860−4866.
4. Barry, J. K., and Matthews, K. S. (1997) *Biochemistry 36,* 15632−15642.
5. Kombo, D. C., Nemethy, G., Gibson, K. D., Ross, A. J. B., Rackovsky, S., and Scheraga, H. A. (1996) *J. Protein Chem. 15,* 77−86.
6. Vos, R., Engelborghs, Y., Izard, J., and Baty, D. (1995) *Biochemistry 34,* 1734−1743.
7. Weitzman, C., Consler, T. G., and Kaback, H. R. (1995) *Protein Sci. 4,* 2310−2318.
8. Szpikowska, B. K., Beechem, J. M., Sherman, M. A., and Mas, M. T. (1994) *Biochemistry 33,* 2217−2225.
9. Mann, C. J., Royer, C. A., and Matthews, C. R. (1993) *Protein Sci. 2,* 1853−1861.
10. Royer, C. A., Mann, C. J., and Matthews, C. R. (1993) *Protein Sci. 2,* 1844−1852.
11. Reece, L. J., Nichols, R., Ogden, R. C., and Howell, E. E. (1991) *Biochemistry 30,* 10895−10904.
12. Nichols, R., Weaver, C. D., Eisenstein, E., Blakley, R. L., Appleman, J., Huang, T.-H., Huang, F.-Y., and Howell, E. E. (1993) *Biochemistry 32,* 1695−1706.
13. Zhuang, P., Eisenstein, E., and Howell, E. E. (1994) *Biochemistry 33,* 4237−4244.
14. Bradrick, T. D., Shattuck, C., Strader, M. B., Wicker, C., Eisenstein, E., and Howell, E. E. (1996) *J. Biol. Chem. 271,* 28031−28037.
15. Matthews, D. A., Smith, S. L., Baccanari, D. P., Burchall, J. J., Oatley, S. J., and Kraut, J. (1986) *Biochemistry 25,* 4194−4204.
16. Amyes, S. G. B., and Gemmel, C. G. (1992) *J. Med. Microbiol. 36,* 4−29.
17. Narayana, N., Matthews, D. A., Howell, E. E., and Xuong, N.-H. (1995) *Nat. Struct. Biol. 2,* 1018−1025.
18. Zieg, J., Maples, V. F., and Kushner, S. R. (1978) *J. Bacteriol. 134,* 958−966.
19. Tartof, K. D., and Hobbs, C. A. (1987) *BRL Focus 9,* 12.
20. Vermersch, P. S., Klass, M. R., and Bennett, G. N. (1986) *Gene 41,* 289−297.
21. Gornall, A. G., Bardawill, C. J., and David, M. M. (1949) *J. Biol. Chem. 177,* 751−766.
22. Howell, E. E., Warren, M. S., Booth, C. L. J., Villafranca, J. E., and Kraut, J. (1987) *Biochemistry 26,* 8591−8598.
23. Ellis, K. J., and Morrison, J. F. (1982) *Methods Enzymol. 87,* 405−426.
24. Cleland, W. W. (1963*) Biochim. Biophys. Acta* 67, 104−137.
25. Zhuang, P., Yin, M., Holland, J. C., Peterson, C. B., and Howell, E. E. (1993) *J. Biol. Chem. 268,* 22672−22679.
26. Dunn, S. M. J., Lanigan, T. M., and Howell, E. E. (1990) *Biochemistry 29,* 8569−8576.
27. Beddard, G. S., Fleming, G. R., Porter, G., and Robbins, R. I. (1980) *Philos. Tran.s R. Soc London A: Math. Phys. Sci. 298,* 321−324.
28. Demchenko, A. P. (1986) *Ultraviolet Spectroscopy of Proteins,* pp 24−24, Springer-Verlag, Berlin and Heidelberg, Germany.
29. Pace, C. N., Shirley, B. A., and Thompson, J. A. (1990) in *Protein Structure: A Practical Approach (*Creighton, T. E., Ed.) pp 311−330, IRL Press, Oxford, England.
30. Prasad, K., Lippoldt, R. E., and Edelhoch, H. (1985) *Biochemistry 24,* 6421−6427.
31. Murray, M. B., Tadaki, D. K., Campion, S. R., Lamerdin, J. A., Serpersu, E. H., Bradrick. T. D., and Niyogi, S. K. (1998) *Protein Eng. 11,* 1041−1050.
32. Provencher, S. W., and Glöckner, J. (1981) *Biochemistry 20,* 33−37.
33. Green, S. M., Knutson, J. R., and Hensley, P. (1990) *Biochemistry 29,* 9159−9168.
34. Woody, R. W. (1995) *Methods Enzymol. 246,* 34−70.
35. Eftink, M. R. (1991) *Methods Biochem. Anal. 35,* 127−205.
36. Park, H., Zhuang, P., Nichols, R., and Howell, E. E. (1997) *J. Biol. Chem. 272,* 2252−2258.
37. Kyte, J., and Doolittle, R. F. (1982) *J. Mol. Biol. 157,* 105−132.
38. Bowie, J. U., Reidhaar-Olson, J. F., Lim, W. A., and Sauer, R. T. (1990) *Science 247,* 1306−1310.
39. Cordes, M. H. J., and Sauer, R. J. (1999) *Protein Sci. 8,* 318−325.

40. Chen, Y., and Barkley, M. D. (1998) *Biochemistry 37*, 9976−9982.
41. Vincent, M., Brochon, J.-C., Merola, F., Jordi, W., and Gallay, J. (1988) *Biochemistry 27*, 8752−8761.
42. Ross, J. B. A., Rousslang, K. W., and Brand, L. (1981) *Biochemistry 20*, 4361−4369.
43. Ross, J. B. A., Schmidt, C. J., and Brand, L. (1981) *Biochemistry 20*, 4369−4377.
44. Davenport, L., Knutson, J. R., and Brand, L. (1986) *Faraday Discuss. Chem. Soc. 81*, 81−94.
45. Davenport, L., Knutson, J. R., and Brand, L. (1986) *Biochemistry 25*, 1186−1195.
46. Eftink, M. R., Wasylewski, Z., and Ghiron, C. A. (1987) *Biochemistry 26*, 8338−8346.
47. Knutson, J. R., Beechem, J. M., and Brand, L. (1983) *Chem. Phys. Lett. 102*, 501−507.
48. Kim, S.-J., Chowdhury, F. N., Stryjewski, W., Younathan, E. S., Russo, P. S., and Barkley, M. D. (1992) *Biophys. J. 65*, 215−226.
49. Creighton, T. E. (1993) *Proteins* W. H. Freemand and Co.: New York; p 4.

BI992195X